PHYSICAL PROPERTIES OF UPPER MIDWEST U.S.-GROWN HYBRID HAZELNUTS

D. R. Bohnhoff, K. S. Lawson, J. A. Fischbach

ABSTRACT. *Nuts from F_1 hybrid hazelnuts grown in Wisconsin were harvested and dried to eight different moisture contents. Nut dimensions and mass were recorded. Nuts were then subjected to uniaxial compression to determine total deformation required for rupture, rupture force, and rupture energy for each of the three major nut axes. Kernel dimensions, shell thickness, shell mass, and kernel mass of each nut were recorded after rupture. Hybrid hazelnuts and kernels were found to be smaller than European varieties. Nut geometry was found to change with nut size. When a nut is loaded, an initial crack forms along a longitudinal line parallel to the direction of applied load and then rapidly propagates until it has extended along two longitudinal lines (both parallel to the applied load), causing the shell to split into two pieces. Under lateral (Y-axis and Z-axis) loadings, the shell is split into nearly identical halves. Loading along the X-axis required the lowest rupture force, rupture energy, and rupture strain of all loading axes. Rupture force, rupture energy, and stiffness were shown to be highly correlated with moisture content. At lower moisture contents, shells fractured into more pieces.*

Keywords. *Hazelnut, Nut cracking, Nut geometry, Nut rupture force, Shelling, Shell thickness.*

Continual development of European hazelnut (*Corylus avellana*) cultivars has resulted in their commercial adoption in various locations worldwide, including the Willamette Valley of Oregon, which is located just inland of the Pacific Ocean in the U.S. Northwest. Unfortunately, most European hazelnut cultivars are susceptible to Eastern Filbert Blight (EFB) and/or lack the cold-hardiness required for cultivation across the Upper Midwest of the U.S. Two species of hazelnut, the American (*C. americana*) and Beaked (*C. cornuta*), are native to and grow well in the Upper Midwest but are not as productive as their European counterpart. By crossing the European hazelnut with American and Beaked species, researchers associated with the Upper Midwest Hazelnut Development Initiative (UMHDI) hope to obtain varieties for the Upper Midwest that are productive, cold-hardy, and disease resistant.

In addition to its primary focus on hybrid hazelnut productivity, cold-hardiness, and disease resistance, the UMHDI is interested in secondary traits such as plant size and shape, kernel quality, and whole nut characteristics. Unlike European hazelnuts, which are generally pruned to grow as trees, Upper Midwest hybrid hazelnuts are being grown as shrubs, thereby requiring a study of plant size and shape for establishment of plant and orchard maintenance practices and mechanical harvester design. Kernel quality includes items such as size and taste that affect consumer demand and potential culinary uses. Whole nut characteristics include drying properties and physical characteristics that dictate approaches to storage and processing, and influence drying and processing equipment selection. Physical characteristics include properties such as moisture content, nut size, nut shape, shell thickness, space between shell and kernel, and cracking force. The ultimate goal of work related to post-harvest storage and processing is the low-cost recovery of high-quality, uncracked, and unchipped kernels with little or no product waste.

The fundamental importance of physical properties to hazelnut processing has prompted several studies on *C. avellana*. Working with the 'Tombul' variety of *C. avellana*, Aydin (2002) measured axial dimensions, unit mass and volume, density, sphericity, porosity, projected area, terminal velocity, rupture strength, and coefficients of static and dynamic friction and determined the moisture content dependency of several of the properties. Güner et al. (2003) studied the effects of moisture content and load direction on specific deformation, rupture force, and rupture energy of the 'Aci Findik', 'Cakildak', 'Tombul', and 'Güney Karasi' cultivars of *C. avellana.* Ozdemir and Akinci (2004) reported on differences in physical properties among the 'Palaz', 'Tombul', 'Cakildak', and 'Kara' varieties of *C. avellana*, slightly before Valentini et al. (2006) examined the effect of load direction on rupture force, rupture energy, and specific deformation of *C. avellana* varieties 'Barcelona', 'Ennis', 'Tonda Bianca', and 'Toda Giffoni'. Ercisli et al. (2011) measured color, axial dimensions, mass, geometric mean diameter, sphericity, surface area, rupture force, deformation, rupture energy, and hardness for three genotypes (K-1/1, K-19/6, and K-24/2) and nine common Turkish cultivars ('Allah verdi', 'Foşa', 'Kargalak', 'Kuş', 'Mincane', 'Sivri', 'Uzun Musa', 'Yassi badem', and 'Yuvarlak badem') of *C. avellana*. Most recently, Delprete and Sesana

Submitted for review in February 2019 as manuscript number PRS 13378; approved for publication as a Research Article by the Processing Systems Community of ASABE in July 2019.

The authors are **David R. Bohnhoff,** Emeritus Professor, Department of Biological Systems Engineering, **K. Scott Lawson,** Undergraduate Student, Department of Civil and Environmental Engineering, and **Jason A. Fischbach,** Agriculture Educator, Extension Ashland County, University of Wisconsin, Madison, Wisconsin. **Corresponding author:** David R. Bohnhoff, 460 Henry Mall, Madison, WI 53706; phone: 608-577-7130; e-mail: bohnhoff@wisc.edu.

  ISSN 2151-0032 https://doi.org/10.13031/trans.13378

(2014) and Delprete et al. (2015) used numerical modeling and physical testing to determine mechanical properties of 'Tonda Gentile Trilobata', an Italian cultivar of *C. avellana*.

Despite extensive physical properties research on *C. avellana*, similar research on *C. americana*, *C. cornuta*, and crosses involving *C. avellana* is extremely limited, and thus the extent to which physical properties are influenced by hazelnut species has not been quantified.

Research Objective

The objective of this research project was to quantify whole nut dimensions, kernel dimensions, shell cracking characteristics, and cracking properties of hybrid hazelnuts grown in the Upper Midwest and to relate specific cracking properties to changes in moisture content, load direction, nut size, and other independent variables.

Materials and Methods

Orthogonal Coordinate System

For experimental purposes, nuts in this study were treated as ellipsoids, with the orthogonal axes shown in figure 1 used to define nut dimensions and loading directions. The coordinate axis containing the poles (i.e., the hazelnut hilum and tip) was established as the X-axis, and the dimension of the nut in this direction was defined as dimension *A*. The Y-axis and Z-axis were situated in the equatorial plane such that they were aligned, respectively, with the major and minor dimensions of the whole nut (not the kernel) within the equatorial plane. Because whole nut dimensions *B* and *C* correspond to dimensions measured along the Y-axis and Z-axis, respectively, whole nut dimension *B* always exceeds the magnitude of dimension *C*.

The coordinate axes established by the whole nut (i.e., the kernel surrounded by its shell) is the same coordinate system used when recording kernel dimensions for the same nut. Given that kernel shape does not exactly match whole nut shape, it is possible for dimension *C* of a particular kernel to exceed its *B* dimension.

With the hilum and tip as poles, the terms longitudinal and latitudinal are herein used to describe nut surface lines in the same manner as cartographers use them to define locations on a globe. In other words, a longitudinal line is one running from the hilum to the tip.

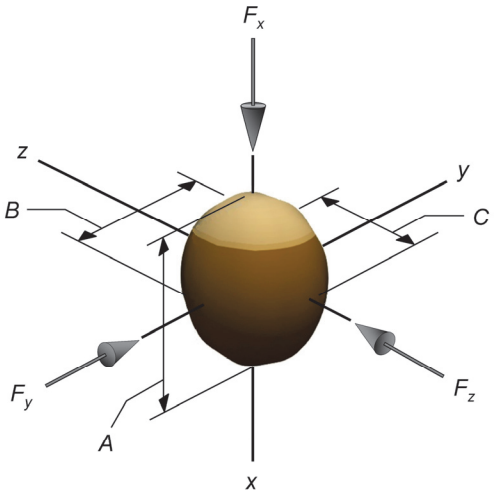

Figure 1. Orthogonal coordinate system.

Experimental Design

To investigate the influence of moisture content and loading direction on cracking characteristics, a full 8 × 3 factorial design (8 moisture content levels × 3 loading directions) was replicated 15 times. More specifically, nuts were conditioned to eight different moisture contents, with 15 nuts at each moisture content level loaded in the X-direction, 15 in the Y-direction, and 15 in the Z-direction.

Source Material

Hazelnut clusters (fig. 2) were hand-harvested on September 1, 2016, from a farm near Stoughton, Wisconsin. This particular planting was established in 2011 using full-sibling F1 seedlings from a controlled-cross block managed by Forest Agriculture Enterprises, Viola, Wisconsin (Fischbach and Tibbals, 2016). The parents for the controlled cross were selected by Forest Agricultural Enterprises from their own mature planting of hybrid hazelnuts. Hazelnut plantings

Figure 2. Hazelnut clusters at various states of maturity.

at Forest Agriculture Enterprises were in turn established using seedlings purchased from Badgersett Research Corporation in Canton, Minnesota. According to Badgersett (2015), their hybrid hazelnut populations include "individuals showing extensive mixtures of the definitive characteristics of the three parent species (American, Beaked, and European), and virtually any combination of traits can either be seen or could likely be generated."

Moisture Conditioning and Measurement

After transport to the University of Wisconsin-Madison Agricultural Engineering Laboratory, clusters from individual shrubs were thoroughly mixed together, and the resulting mixture was separated into 18 groups, with each group dried to a different moisture content. This moisture content conditioning was achieved by placing clusters above saturated salt solutions in specially fabricated, biomaterial moisture conditioning (BMC) units (Bohnhoff, 2017). Six different saturated salt solutions were used, with the BMC units maintained at three different temperatures. After three months, a portion of material from each of the 18 BMC units was removed, analyzed, and used to establish moisture desorption isotherms for husks, shells, and kernels of the hybrid hazelnuts (Bohnhoff and Bohnhoff, 2019). Once the desorption research was completed, additional clusters were removed from eight of the BMC units for use in this study. The eight BMC units were selected to provide a broad range of nut moisture contents. Each group was assigned a moisture content (MC) group number 1 through 8.

Immediately after removal from their BMC unit, clusters were dehusked by hand and visually inspected. Nuts showing any insect or physical damage were removed. The remaining nuts were immediately placed in a sealed, 1 L storage bottle labeled to identify their MC group number. After 24 h, the nuts were considered to have reached a new equilibrium within their respective bottles, and testing began. Roughly 100 g of whole nuts were removed from a storage bottle, rapidly hand-cracked, separated into shells and kernels, and each fraction was immediately weighed using a digital scale with a resolution 0.001 g. This process was repeated with a 100 g sample from each bottle. Shell and kernel fractions were then oven-dried at 103°C ±2°C for 48 h (Bohnhoff, 2017; Bohnhoff and Bohnhoff, 2019; Palipane and Driscoll, 1992) and reweighed. Kernel and shell mass ratios and kernel and shell moisture contents were then calculated for each MC group.

Nut and Kernel Dimensions and Related Properties

Measurement of whole nut dimensions, cracking characteristics, and kernel dimensions was started as soon as the nuts were considered to have reached equilibrium within their respective storage bottles. This was done one nut at a time to minimize moisture content changes by minimizing the elapsed time a nut was outside its storage bottle prior to compression testing. A digital caliper with 0.01 mm resolution was used to obtain whole nut and kernel dimensions. Whole nut dimensions were measured just prior to compression testing, and kernel measurements were measured just after testing. Geometric mean diameter (D_P), percentage sphericity (ϕ), and shape index (SI) were then calculated from whole nut and kernel dimensions.

An object's geometric mean diameter is defined as the diameter of a sphere that has the same volume as the object. The volume of an irregularly shaped object is generally obtained by measuring the volume of fluid the object displaces. In the case of hazelnuts, researchers frequently treat the whole nut (or kernel) as a perfect ellipsoid, with whole nut (or kernel) dimensions A, B, and C treated as the three principal dimensions of a perfect ellipsoid. When this is done, the volume of the whole nut (or kernel) is given as $\pi ABC/6$, and the geometric mean diameter becomes:

$$D_P = (ABC)^{1/3} \quad (1)$$

Sphericity is a measure of how closely the shape of an object approaches that of a perfect sphere and is defined as the ratio of the object's volume to that of a circumscribing sphere. A circumscribing sphere is the smallest perfect sphere that can completely encase the object. When an object is treated as a perfect ellipsoid with principle dimensions A, B, and C, the percentage sphericity of the object is given as:

$$\phi = 100(ABC)^{1/3}/L = 100D_P/L \quad (2)$$

where L is the larger of dimensions A, B, and C.

The shape index (SI) of a whole nut (or kernel) is equal to the average of the major and minor dimensions within the equatorial plane (i.e., dimensions B and C) divided by the dimension measured along the polar axis (i.e., dimension A). In equation form:

$$SI = (B + C)/(2A) \quad (3)$$

Compression Tests and Cracking Characteristics

Compression tests were performed using a 5 kN MTS Insight Electromechanical Testing System (MTS, Eden Prairie, Minn.). Load was applied at a rate of 1.25 mm min^{-1} in accordance with ASABE Standard S368.4 (ASABE, 2017). To prevent nuts from rolling during X-direction loading, each X-direction-loaded nut was lightly sanded along its compressed ends (fig. 3). This was thought to have only a minor influence on rupture strength.

Once rupture strength was reached, the nut was removed from the machine, and the shell was pulled apart. In some cases, shells were pried apart with a razor blade to fully release the kernel. Shell fragmentation information was then collected, kernel dimensions and shell thickness were measured, and shell and kernel mass were recorded. Some nuts lacked kernels, and some kernels were shattered during nut rupture, thereby thwarting measurement of their dimensions.

To quantify shell fragmentation, ruptured shell fragments from a particular nut were placed into four size categories based on a visual estimation of initial whole nut surface area. Specifically, each fragment was categorized as being greater than 1/2 of the whole nut surface area, between 1/2 and 1/3 of the whole nut surface area, between 1/3 and 1/4 of the whole nut surface area, or less than 1/4 of the whole nut surface area. The number of shell fragments in each size category was recorded for each nut.

For each load test, a rupture force (P_R), initial stiffness

Figure 3. Nuts sanded for compression along the X-axis.

(K_I), secant stiffness (K_S), rupture energy (E_R), and nut deformation at rupture (Δ_R) were obtained from the load-displacement curve (fig. 4). Initial stiffness was first calculated by taking the slope of the load-displacement curve between 90 and 180 N (20 and 40 lbf). The point at which this initial stiffness line crossed the *x*-axis was defined as the load head displacement associated with zero nut deformation (identified as X_0 in fig. 4). This extrapolation of the initial stiffness line removes initial portions of the recorded load-displacement curve associated with (1) removal of slack in the top platen mounting linkage as the nut makes contact with the 2.3 kg (5 lbm) top platen, (2) initial nut "seating" and/or repositioning between load platens, and (3) slight rotation of both platens as the top platen contacts the nut. Load head displacement associated with rupture (X_R) and rupture force (P_R) are the *x*-*y* coordinates of the rupture point, which was defined as the point at which the greatest force was attained during loading. The difference between X_R and X_0 is nut deformation at rupture (Δ_R). Secant stiffness is numerically equal to the rupture force divided by the nut deformation at rupture, and rupture energy is equal to the area under the load-displacement curve between X_0 and X_R. Obtaining these cracking characteristics from the load-displacement curve was independently accomplished using (1) a specially written FORTRAN program, and (2) R statistical analysis software (R Development Team, 2016).

The ratio of nut deformation at rupture (Δ_R) to the nut's undeformed dimension in the direction of loading (l) is referred to as specific deformation by some researchers but is herein referred to as rupture strain (ε). When expressed as a percentage, rupture strain is calculated as:

$$\varepsilon\ (\%) = \Delta_R / l \times 100 \quad (4)$$

where l is whole nut dimension A for X-axis loading, dimension B for Y-axis loading, and dimension C for Z-axis loading.

Kernel Density

After all compression tests were completed, the density of a crushed sample of hybrid hazelnut kernels was determined using an Isolab 100 mL calibrated glass pycnometer (Isolab, Eschau, Germany) and water.

Results and Discussion

Data Source

Individual measurements for all whole nuts, their shells, and their kernels were provided by Lawson et al. (2018). This includes mass and dimensional data for each whole nut and kernel; rupture force, initial stiffness, secant stiffness, deformation at rupture, and rupture strain for each whole nut; and shell thickness and shell fragmentation data.

Of the 360 nuts tested, eight (slightly over 2%) did not contain a kernel. Although nuts with noticeable insect damage were culled from the study prior to testing, it is not known if missing kernels in the tested nuts were the result of insect damage or plant genetics. When compiling statistics on kernels, the eight nuts without kernels were removed from the data set (i.e., the kernels were not assigned masses and dimensions of zero and then included in the data set).

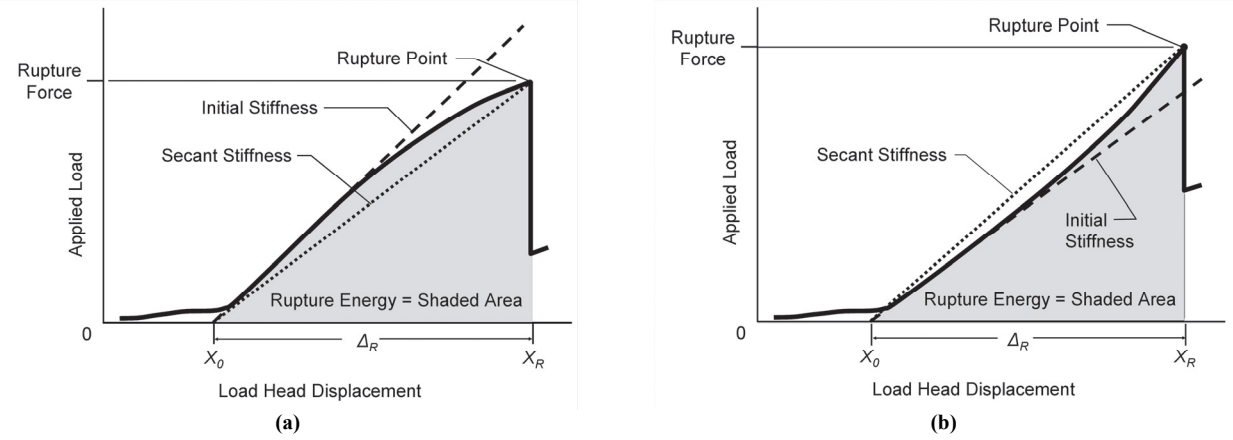

Figure 4. Load-displacement curves and associated cracking characteristics.

Moisture Content

Moisture content values and mass ratios for each moisture content (MC) group are compiled in table 1. Nuts in MC groups 3 and 8 were conditioned at about 2°C, while those in the other MC groups were conditioned at 23°C. Nuts in MC group 7 exhibited some mold growth, which was not surprising, as they were maintained in a room temperature environment at a relative humidity near 85%. This mold was assumed to have an insignificant effect on cracking characteristics.

Nut and Kernel Geometry

Probability distribution curves for whole nut and kernel dimensions are shown in figure 5. Table 2 contains statistics corresponding to these distributions along with similar statistics for *C. avellana* (European hazelnuts) collected by Italian and Turkish researchers and compiled by Lawson et al. (2018). Table 3 contains statistics for geometric mean diameter, mass, and sphericity of whole nuts and kernels for both hybrid and European hazelnuts. Table 4 contains a categorization of whole nut dimensions by relative size. In table 4, the largest, middle, and smallest whole nut dimensions are identified as S1, S2, and S3, respectively. Because, by definition, whole nut dimension *B* is always larger than whole nut dimension *C*, whole nut dimension *B* can never be the smallest dimension (S3), and whole nut dimension *C* can never be the largest dimension (S1). Additionally, the only time that whole nut dimension *C* is not the smallest dimension is when whole nut dimension *A* is the smallest dimension.

The data in table 2 show that dimension *B* for whole nuts has a slightly greater mean value than dimension *A*, but the variation in dimension *A* for whole nuts is less than that for dimension *B*. Any nut whose *B* dimension exceeds its *A* dimension would be described as being more oblate. As indicated in table 4, 58.3% of whole nuts had an *A* dimension that was exceeded by its *B* dimension but not its *C* dimension, and 11.9% of whole nuts had an *A* dimension that was exceeded by both its *B* and *C* dimensions.

A plot of whole nut dimensions versus geometric mean diameter (fig. 6) clearly shows that hybrid hazelnuts tend to become more oblate as they increase in overall size. Figure 6 shows that dimensions *B* and *C* both increase at similar rates relative to overall nut size. Relative to dimensions *B* and *C*, dimension *A* increases at a lower rate relative to overall nut size, which explains the lower relative coefficient of variation for dimension *A*.

The greater the shape index, the more likely a nut is to be oblate, and any nut with a shape index greater than 1.0 would be defined as oblate. To this end, the plot of shape index ver-

Table 1. Shell and kernel mass ratios and moisture contents.

MC Group	Mass Percentage (% w.b.)		Moisture Content (% d.b.)		
	Shells	Kernels	Shells	Kernels	Whole Nuts
1	66.6	33.4	7.8	2.9	6.2
2	64.6	35.4	9.3	3.7	7.3
3	66.1	33.9	10.3	4.2	8.2
4	67.8	32.2	16.6	5.9	13.2
5	68.6	31.4	16.6	5.4	13.1
6	67.9	32.1	17.4	5.8	13.7
7	67.5	32.5	21.0	6.8	16.4
8	69.2	30.8	24.0	7.4	18.9

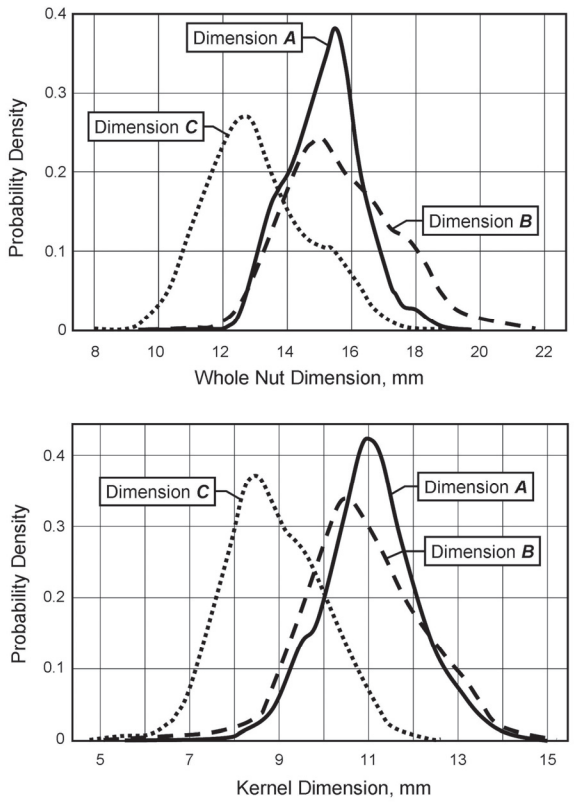

Figure 5. Dimension distributions for hybrid hazelnuts.

Table 2. Whole nut and kernel size dimension statistics (SD = standard deviation, and CV = coefficient of variation).

Statistic	Whole Nut Dimensions (mm)			Kernel Dimensions (mm)		
	A	*B*	*C*	*A*	*B*	*C*
Upper Midwest hybrid hazelnuts						
Mean	15.17	15.71	13.56	10.56	10.41	8.47
SD	1.14	1.68	1.65	2.49	2.52	2.08
CV (%)	7.5	10.7	12.2	23.6	24.2	24.5
European hazelnuts (*C. avellana*)[a]						
Mean	21.21	19.25	18.01	16.00	13.77	12.78
SD	2.75	2.67	2.98	2.44	1.34	2.02
CV (%)	13.0	13.9	16.5	15.2	9.7	15.8

[a] From data compiled by Lawson et al. (2018).

Table 3. Whole nut and kernel size, mass, and shape distribution statistics (D_P = geometric mean diameter, and ϕ = sphericity).

Statistic	Whole Nut			Kernel		
	D_P (mm)	Mass (g)	ϕ (%)	D_P (mm)	Mass (g)	ϕ (%)
Upper Midwest hybrid hazelnuts						
Mean	14.76	1.53	92.1	10.16	0.49	88.3
SD	1.32	0.45	3.2	0.99	0.16	4.8
CV (%)	8.9	29.1	3.4	9.8	31.9	5.4
European hazelnuts (*C. avellana*)[a]						
Mean	19.38	2.63	90.0	14.06	1.18	87.7
SD	2.31	0.80	7.2	1.43	0.26	9.1
CV (%)	11.9	30.2	8.0	10.1	21.7	10.4

[a] From data compiled by Lawson et al. (2018).

Table 4. Relative size ranking of whole nut dimensions.

Whole Nut Dimension	Frequency in Size Category (%)		
	Largest (S1)	Middle (S2)	Smallest (S3)
A	41.7	46.4	11.9
B	58.3	41.7	0
C	0	11.9	88.1

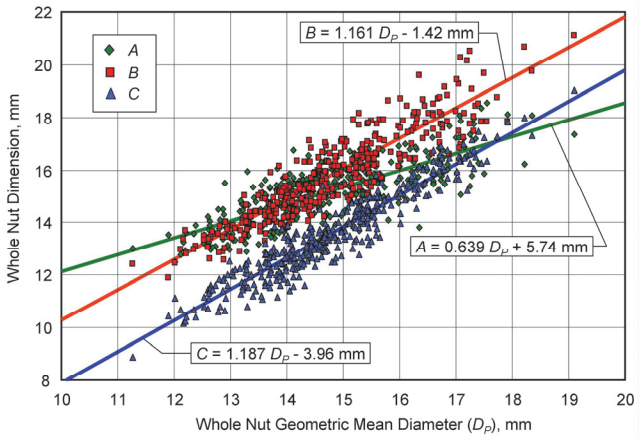

Figure 6. Whole nut dimensions as a function of geometric mean diameter.

sus geometric mean diameter for whole nuts in figure 7 also supports the conclusion that larger hybrid hazelnuts tend to be more oblate.

In general, comparisons between mean values for hybrid and European hazelnuts in tables 2 and 3 can be made on the basis that each data set represents a collection of different genotypes. That said, the data set for European hazelnuts is largely comprised of varieties that were selected and are being cloned and grown because of specific traits, including size. This is in sharp contrast to the plants that produced the hybrid hazelnuts, all of which were grown from seed, and none of which are currently slated for propagation. This explains a portion of the significant size difference between European and hybrid nuts. As given in table 3, the mean geometric diameter (D_P) of 19.4 mm for European whole nuts exceeded the corresponding hybrid value of 14.8 mm by 31%, whereas the D_P value of 14.1 mm for European kernels exceeded the corresponding hybrid value of 10.2 mm by 38%.

Inasmuch as kernel mass is directly related to kernel volume, and kernel volume is approximated by $\pi/6$ times the cube of geometric mean diameter, a measurable difference in kernel size translates into a significant difference in kernel mass. Stated differently, the cube of the D_P ratio roughly approximates the difference in mass. In this case, the cube of the European to hybrid kernel D_P ratio is $(14.1/10.2)^3 = 2.64$. The actual ratio of kernel masses is $(1.18/0.49) = 2.41$. This fundamental disparity in mass is driving researchers to cross *C. americana* and *C. cornuta* with *C. avellana* to obtain a larger nut.

Sphericity values for hybrid whole nuts and kernels (table 3, fig. 8) were not found to be a function of size. Mean sphericity of both were similar to those reported for European varieties. Hybrid kernel sphericity values are also similar to those reported by Braun et al. (2019) or the Upper Midwest hybrid hazelnuts they examined.

Size Sorting

Size sorting is accomplished with equipment that contains a physical barrier with openings. Although processors tend to focus on the cost and throughput capacity of this equipment, the shape of the openings is just as important. As shown in figure 9, an elongated opening, like a slot, will sort objects using their smallest dimension (i.e., S3), whereas a barrier with round holes will sort objects using their middle (i.e., S2) dimension. Barriers with elongated openings are generally used prior to cracking for purposes that will be ex-

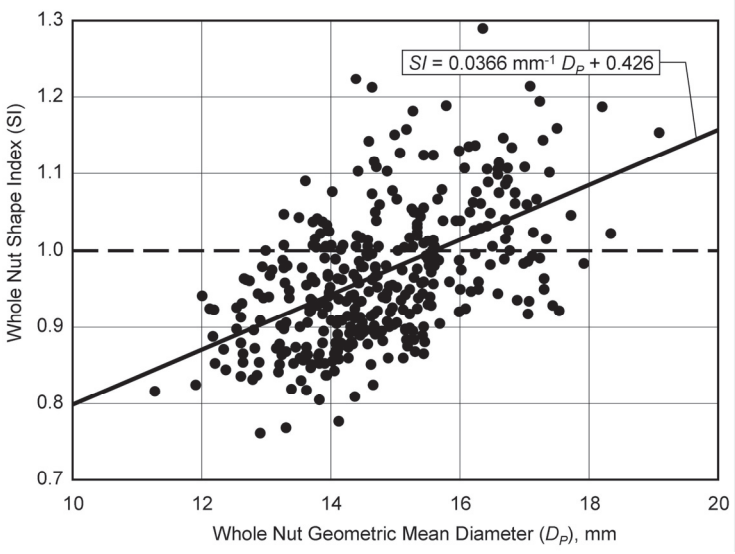

Figure 7. Shape index versus geometric mean diameter for whole nuts.

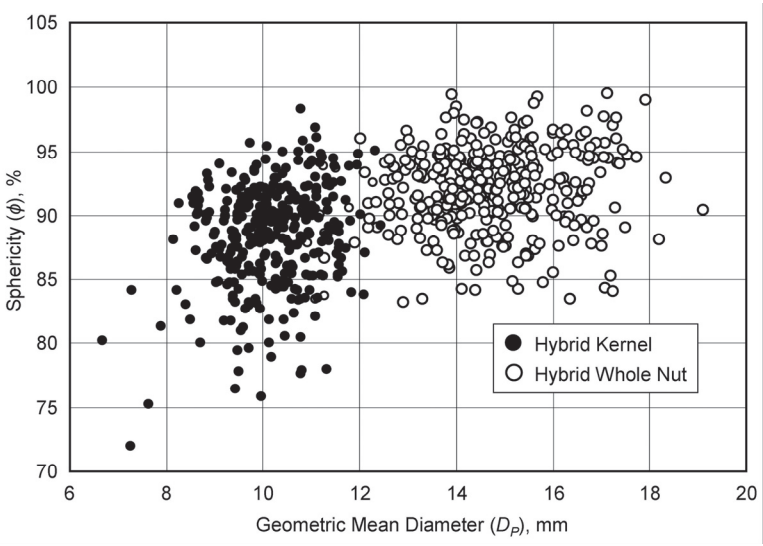

Figure 8. Sphericity of hybrid whole nuts and kernels as a function of geometric mean diameter.

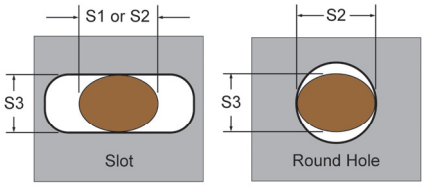

Figure 9. Barriers with slots (left) sort objects based on their smallest dimension (S3). Barriers with round holes (right) sort objects based on their middle dimension (S2).

plained later. Separation of kernels from shell fragments uses barriers with slots that are narrower than the S3 dimension of the kernels, with the narrower shell fragments passing through the barrier. Large shell fragments that are not removed by this operation can generally be separated from the kernels using a barrier with round holes whose diameter just exceeds that of the kernel's middle (i.e., S2) dimension. In this case, the kernels pass through the barrier.

Shell Fracture Characteristics

Failure Mode

Almost without exception, an initial crack formed along a longitudinal line parallel to the direction of applied load. As previously noted, with the hilum and tip of a whole nut as the poles, the term "longitudinal" is used to describe nut surface lines in the same manner as cartographers use it to define locations on a globe. In other words, a longitudinal line is one running from the hilum to the tip, and each curved longitudinal line lies in a unique plane that includes the poles of the nut.

Cracking along a longitudinal line is not surprising because cracks also form along longitudinal lines during rapid nut drying, an indication of a fundamental weakness in the lateral direction. To what extent this inherent weakness is due to the type, shape, size, orientation, and/or alignment of cells, or abrupt changes in any of these characteristics, was not examined. The fact that shell surfaces are characterized by slight color striations that run parallel to longitudinal lines is an indication of a longitudinal arrangement of cells. A weakness perpendicular to this direction is consistent with the wood of stems and roots, which is weakest in tension perpendicular to its fiber (i.e., grain) direction (FPL, 2010).

Once a crack forms under load, it propagates rapidly until it has extended along two longitudinal lines, causing the shell to split into two pieces. Additional deformation past this rupture point typically results in more fragmentation of the shell and/or crushing of the kernel. For nuts loaded parallel to the Y-axis, the two longitudinal lines along which the shell splits are nearly coplanar and closely aligned with the X-Y plane of the nut (fig. 10). Likewise, for nuts loaded parallel to the Z-axis, the two longitudinal lines are nearly coplanar and closely aligned with the nut's X-Z plane (fig. 10). In other words, under Y-axis and Z-axis loadings, the shell is split into nearly identical halves (fig. 11). This occurs because a nut oriented with its X-axis perpendicular to the direction of loading has only two longitudinal lines that lie in a vertical plane, and these two lines (one on the top side of the nut and one on the bottom side of the nut under a vertical load) lie in the same vertical plane.

Nuts under X-axis loading are less likely to split into two nearly identical halves because, in theory, an infinite number of longitudinal lines lie in a vertical plane. As shown in figure 12, it is not uncommon for the shell of an X-axis loaded nut to fracture into two pieces that vary in size by 100%. In all four cases, the two longitudinal lines involved in the fracture are far from coplanar. The downside of these very asymmetrical fractures is that the kernel is often locked inside the larger shell fragment.

Shell Fragmentation

The degree of shell fragmentation due to cracking is an important parameter in the subsequent separation of shell fragments from kernels. Generally, the more pieces into which a shell fractures, the greater the number of smaller shell fragments. Smaller shell fragments tend to be more difficult to separate from the mix of shell fragments and whole and split kernels. Figure 13 shows the percentage of shells that fractured into more than two pieces as a function of shell moisture content. It is clear from this plot that the drier the shell, the greater the degree of shell fragmentation.

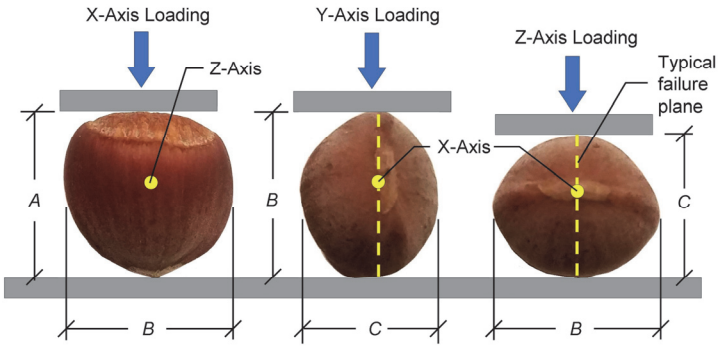

Figure 10. The same nut in each of three loading positions. Typical rupture planes for Y-axis and Z-axis loadings shown with dashed lines.

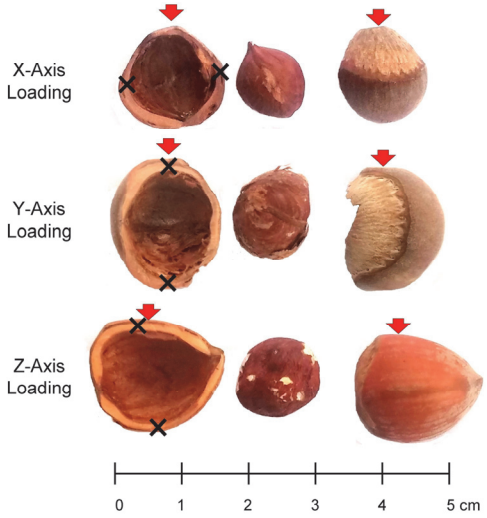

Figure 11. Results of three tests randomly selected for each load direction. Each shell has been split nearly in half. Symbols (×) indicate the intersection of the rupture plane with the nut's equatorial plane.

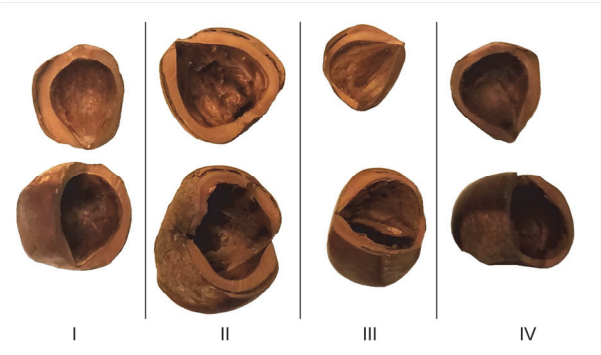

Figure 12. Two unequal-sized shell fragments for each of four X-axis loaded nuts.

Shell Thickness

It is clear from the images in figures 11 and 12 that shell thickness can vary significantly along a single longitudinal line, with a sharp decrease in thickness occurring at the poles. For lack of a simple, effective method to account for this variation in thickness, a decision was made to quantify shell thickness with a single measurement made at the intersection of the rupture plane and equatorial plane (i.e., at locations marked with "×" symbols in fig. 11). For Y-axis loadings, this resulted in shell thickness being measured very near the intersection of the theoretical Y-axis and the equatorial plane. Likewise for Z-axis loadings, shell thickness was measured very near the intersection of the theoretical Z-axis and the equatorial plane.

Mean shell thickness for X-, Y-, and Z-axis loadings were 1.89, 1.63, and 2.01 mm, with associated standard deviations of 0.42, 0.32, and 0.48 mm, respectively. Each of these mean values is based on 120 tests, which makes the difference in mean shell thickness for Y-axis and Z-axis loadings significant at the 0.0001 level. This implies that in addition to variation along longitudinal lines, shell thickness varies around the equatorial plane and is thickest along the minor diameter of the equatorial plane. A probability density curve of shell thickness for each loading axis is plotted in figure 14. If shell thickness values for Y-axis and Z-axis loadings represent the extreme differences in thickness in the equatorial plane, then the curve for shell thickness associated with X-axis loadings would be expected to lie between the curves for Y-axis and Z-axis loadings, as it does in figure 14.

Cracking Properties

Mean values and corresponding coefficient of variation (CV) values for rupture force, rupture energy, initial stiffness, secant stiffness, nut deformation at rupture, and rupture strain are compiled in table 5 for each loading direction. Statements regarding the significance of differences in mean values with load direction are provided in the table footnotes.

The dependencies of each of the six cracking characteristics in table 5 (i.e., rupture force, rupture energy, initial stiffness, secant stiffness, nut deformation at rupture, and rupture strain) on shell thickness, shell moisture content, and mean geometric diameter of the nut were investigated using linear least-squares regression of the cracking characteristics on each of the three properties. The results of these regression analyses are compiled in table 6. The eighth column in table 6 provides the cumulative probability of F(1, 118) distribution associated with the calculated f-value in the seventh column. The greater this probability, the more likely there is a significant relationship between the independent and dependent variables.

Rupture Force

Mean rupture forces for X-, Y-, and Z-axis loadings were 399, 530, and 484 N, respectively (table 5). Using two-tailed t-tests, these mean rupture values are all significantly different at the 0.05 critical alpha level. The regression results in

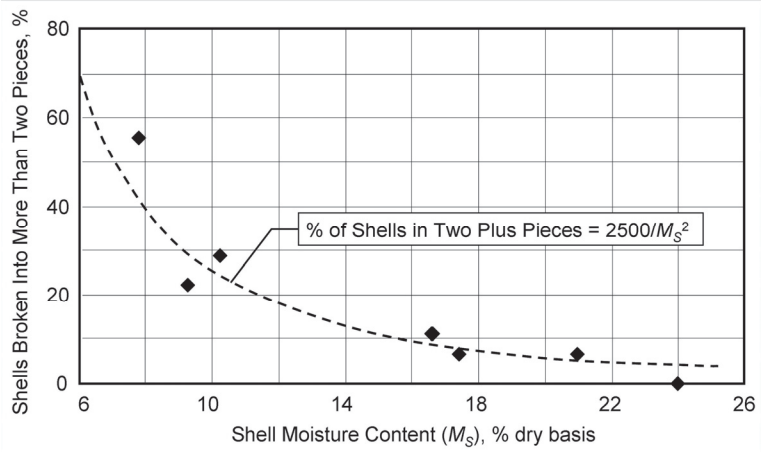

Figure 13. Shell fragmentation versus shell moisture content.

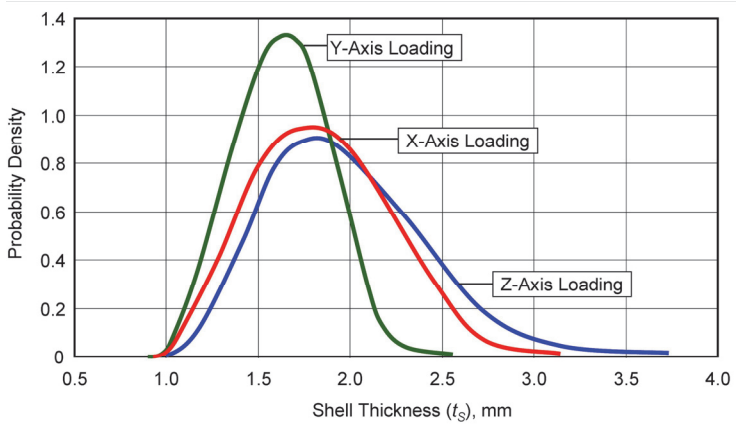

Figure 14. Probability density curves for shell thickness.

Table 5. Mean values and associated coefficient of variations (CV) for cracking properties.

Loading Axis	Rupture Force (P_R)[a] Mean (N)	CV (%)	Rupture Energy (E_R)[b] Mean (J)	CV (%)	Initial Stiffness (K_I)[c] Mean (N mm^{-1})	CV (%)	Secant Stiffness (K_S)[c] Mean (N mm^{-1})	CV (%)	Nut Deformation at Rupture (Δ_R)[a] Mean (mm)	CV (%)	Rupture Strain (ε)[a] Mean (%)	CV (%)
X	399	35.3	0.142	48.6	679	33.5	630	37.0	0.665	26.9	4.4	26.8
Y	530	31.9	0.249	51.6	729	24.0	650	25.6	0.827	25.2	5.4	24.7
Z	484	32.0	0.229	58.7	547	29.2	557	29.8	0.914	36.0	6.1	36.7

[a] For rupture force, rupture strain, and nut deformation at rupture, all three mean values are significantly different at the 0.05 critical alpha level (using two-tailed t-tests).

[b] For rupture energy, the mean value for X-axis loadings is significantly different at the 0.05 critical alpha level from the means for Y-axis and Z-axis loadings. However, the means for Y-axis and Z-axis loadings are not significantly different at the 0.05 critical alpha level.

[c] For initial and secant stiffness, the mean values for Z-axis loadings are significantly different at the 0.05 critical alpha level from the means for X-axis and Y-axis loadings. However, the means for X-axis and Y-axis loadings are not significantly different at the 0.05 critical alpha level.

table 6 show a positive correlation between rupture force and shell thickness, a strong negative correlation between rupture force and shell moisture content, and a weak positive correlation between rupture force and geometric mean diameter. The relationships between rupture force and shell thickness in table 6 are plotted for each loading axis in figure 15. The negative relationship between rupture force and moisture content for each loading axis is shown in figure 16.

The negative correlation between rupture force and moisture content is consistent with the mechanical properties of wood. In general, wood strength and stiffness properties show a linear decrease from low moisture contents (~3% to 5% dry basis) to a moisture content (M_P) slightly less than the fiber saturation point (FPL, 2010). Depending on the particular wood species and mechanical property, values of M_P typically range between 21% and 28% dry basis. As moisture contents increases above M_P, the magnitude of mechanical properties remain unchanged and are referred to as "green" properties. Based on figure 15, it can be concluded that M_P for the rupture force of hazelnuts is between 20% and 25% dry basis.

In general, the relationship between a wood mechanical property and the wood's moisture content can be expressed as:

$$P = P_{max} - (P_{max} - P_G)M/M_P \text{ for } M \le M_P \qquad (5)$$

Table 6. Results of individual regression analyses.

Dependent Variable	Independent Variable	Load Direction	Parameters for Linear Relationship		R^2		$F(1, \nu, f)$[c]	Standard
			Slope[a]	Y-Intercept	Value	f-Value[b]	(%)	Error
Rupture force (P_R, N)	Shell thickness (mm)	X	95.4 N mm^{-1}	218 N	0.08	10.3	99.83	135 N
		Y	245.3 N mm^{-1}	130 N	0.21	31.5	~100	151 N
		Z	127.6 N mm^{-1}	228 N	0.15	21.6	~100	143 N
	Shell moisture content (% d.b.)	X	-14.7 N %M_{db}^{-1}	625 N	0.32	56.6	~100	116 N
		Y	-17.6 N %M_{db}^{-1}	800 N	0.32	55.1	~100	140 N
		Z	-9.5 N %M_{db}^{-1}	631 N	0.11	14.9	99.98	147 N
	Geometric mean diameter (D_P, mm)	X	35.4 N mm^{-1}	-127 N	0.11	14.8	99.98	133 N
		Y	37.2 N mm^{-1}	-21 N	0.07	9.1	99.69	163 N
		Z	23.1 N mm^{-1}	146 N	0.04	5.4	97.8	152 N
Rupture energy (E_R, J)	Shell thickness (mm)	X	0.0361 J mm^{-1}	0.073 J	0.048	5.97	98.4	0.067 J
		Y	0.1026 J mm^{-1}	0.082 J	0.064	8.03	99.5	0.125 J
		Z	0.0815 J mm^{-1}	0.066 J	0.083	10.7	99.86	0.130 J
	Shell moisture content (% d.b.)	X	-0.00396 J %M_{db}^{-1}	0.203 J	0.097	12.7	99.95	0.066 J
		Y	-0.01114 J %M_{db}^{-1}	0.420 J	0.221	33.5	~100	0.114 J
		Z	-0.00534 J %M_{db}^{-1}	0.312 J	0.046	5.72	98.2	0.132 J
	Geometric mean diameter (D_P, mm)	X	0.0109 J mm^{-1}	-0.021 J	0.044	5.44	97.9	0.068 J
		Y	0.0152 J mm^{-1}	0.024 J	0.021	2.49	88.3	0.128 J
		Z	0.0122 J mm^{-1}	0.051 J	0.016	1.92	83.2	0.134 J
Initial stiffness (K_I, N mm^{-1})	Geometric mean diameter (D_P, mm)	X	32.15 N mm^{-2}	201 N mm^{-1}	0.035	4.30	96.0	224 N mm^{-1}
		Y	30.12 N mm^{-2}	283 N mm^{-1}	0.044	5.39	97.8	172 N mm^{-1}
		Z	16.88 N mm^{-2}	300 N mm^{-1}	0.022	2.65	89.4	159 N mm^{-1}
	Shell moisture content (% d.b.)	X	-27.13 N (mm %M_{db})$^{-1}$	1096 N mm^{-1}	0.419	85.2	~100	174 N mm^{-1}
		Y	-16.46 N (mm %M_{db})$^{-1}$	982 N mm^{-1}	0.260	41.4	~100	151 N mm^{-1}
		Z	-5.54 N (mm %M_{db})$^{-1}$	632 N mm^{-1}	0.035	4.33	96.0	158 N mm^{-1}
	Shell thickness (mm)	X	92.1 N mm^{-2}	505 N mm^{-1}	0.029	3.49	93.6	225 N mm^{-1}
		Y	235.6 N mm^{-2}	345 N mm^{-1}	0.181	26.0	~100	159 N mm^{-1}
		Z	44.6 N mm^{-2}	458 N mm^{-1}	0.018	2.14	85.4	159 N mm^{-1}
Secant stiffness (K_S, N mm^{-1})	Geometric mean diameter (D_P, mm)	X	48.91 N mm^{-2}	-96 N mm^{-1}	0.077	9.89	99.8	225 N mm^{-1}
		Y	43.89 N mm^{-2}	1 N mm^{-1}	0.103	13.5	99.96	159 N mm^{-1}
		Z	25.30 N mm^{-2}	187 N mm^{-1}	0.046	5.64	98.1	163 N mm^{-1}
	Shell moisture content (% d.b.)	X	-26.62 N (mm %M_{db})$^{-1}$	1040 N mm^{-1}	0.384	73.5	~100	184 N mm^{-1}
		Y	-13.80 N (mm %M_{db})$^{-1}$	862 N mm^{-1}	0.202	29.4	~100	150 N mm^{-1}
		Z	-8.28 N (mm %M_{db})$^{-1}$	685 N mm^{-1}	0.073	9.30	99.7	161 N mm^{-1}
	Shell thickness (mm)	X	122.1 N mm^{-2}	400 N mm^{-1}	0.048	5.95	98.4	228 N mm^{-1}
		Y	288.7 N mm^{-2}	180 N mm^{-1}	0.300	50.6	~100	140 N mm^{-1}
		Z	85.0 N mm^{-2}	386 N mm^{-1}	0.060	7.51	99.3	162 N mm^{-1}
Nut deformation at rupture (Δ_R, mm)	Shell thickness (mm)	X	0.0299	0.609 mm	0.005	0.58	55.2	0.179 mm
		Y	0.0287	0.780 mm	0.002	0.22	36.3	0.209 mm
		Z	0.1253	0.662 mm	0.033	4.03	95.3	0.325 mm
	Shell moisture content (% d.b.)	X	0.00695 mm %M_{db}^{-1}	0.558 mm	0.045	5.50	97.9	0.175 mm
		Y	-0.0101 mm %M_{db}^{-1}	0.983 mm	0.069	8.79	99.6	0.202 mm
		Z	-0.00396 mm %M_{db}^{-1}	0.975 mm	0.004	0.50	52.1	0.330 mm
	Geometric mean diameter (D_P, mm)	X	-0.00077	0.677 mm	3E-05	0.004	5.0	0.180 mm
		Y	0.00407	0.767 mm	0.0006	0.06	20.3	0.210 mm
		Z	0.00893	0.783 mm	0.001	0.17	32.0	0.330 mm
Rupture strain (ε)	Shell thickness (mm)	X	-0.0399% mm^{-1}	4.51%	0.0002	0.02	12.1	1.19%
		Y	-0.2236% mm^{-1}	5.75%	0.003	0.33	43.6	1.33%
		Z	0.4947% mm^{-1}	5.11%	0.011	1.32	74.8	2.24%
	Shell moisture content (% d.b.)	X	0.0407% %M_{db}^{-1}	3.81%	0.034	4.21	95.7	1.17%
		Y	-0.0577% %M_{db}^{-1}	6.27%	0.055	6.93	99.0	1.30%
		Z	-0.0315% %M_{db}^{-1}	6.59%	0.006	0.69	59.2	2.25%
	Geometric mean diameter (D_P, mm)	X	-0.2002% mm^{-1}	7.41%	0.050	6.17	98.6	1.16%
		Y	-0.1653% mm^{-1}	7.83%	0.023	2.77	90.1	1.31%
		Z	-0.1911% mm^{-1}	8.90%	0.014	1.71	80.6	2.24%

[a] %M_{db} is a unit (not a variable) equal to 1.0% moisture content, dry basis.
[b] Ratio of mean square due to regression to mean square due to residual.
[c] Cumulative probability of F(1, ν) distribution associated with the calculated f-value where ν = 118.

where P is the mechanical property at moisture content M, P_{max} is the mechanical property at $M = 0$, P_G is the mechanical property in the green state, and M_P is the lowest moisture content associated with P_G. The quantity $(P_{max} - P_G)/M_P$ is a constant herein referred to as the moisture content reduction factor (R_M). Substitution of R_M into equation 5 yields:

$$P = P_{max} - R_M M \text{ for } M \le M_P \quad (6)$$

Studies on the behavior of ideal, linear-elastic, thin-shelled spheres under uniaxial compressive loads (Updike and Kalnins, 1970, 1972; Taber, 1983; Shorter et al., 2010) have demonstrated the complex behavior of such objects. Because the behavior of a hazelnut under uniaxial compressive load is much more complex (because of nonlinear and anisotropic shell properties, variable shell thickness, complex overall shape, etc.), no attempt was made to formulate theoretical or semi-theoretical relationships between rupture force and other hazelnut properties. Instead, multivariable regression models for rupture force as a linear function of geometric mean diameter, shell moisture content, shell

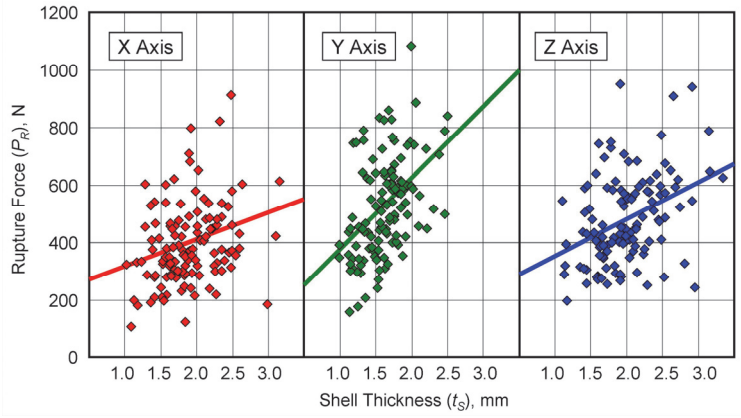

Figure 15. Rupture force as a function of loading axis and shell thickness.

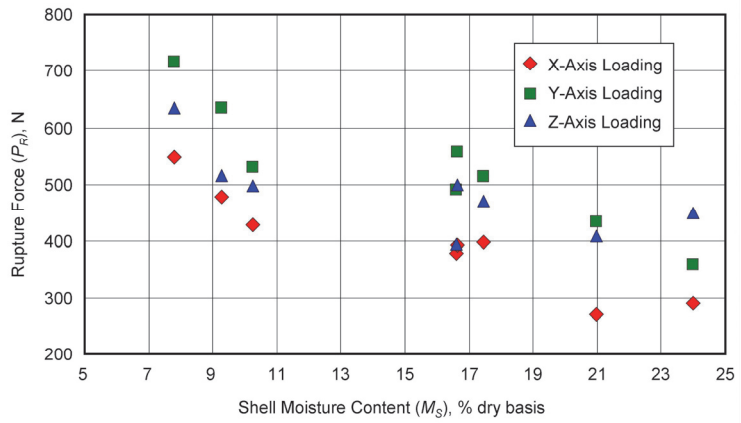

Figure 16. Rupture force as a function of loading axis and shell moisture content. Each data point is the mean of 15 compression tests.

thickness, and the products and quotients of these three independent variables were investigated. These analyses found that residual errors were not significantly reduced with inclusion in the regression models of geometric mean diameter or the products and quotients of the three independent variables. More specifically, the best regression models were the following three-parameter equations with only shell thickness and shell moisture content as independent variables:

X-axis loading:

$$P_R = 426\ \text{N} + t_S\,(111\ \text{N mm}^{-1}) - M_S\,(15.4\ \text{N \%M}_{db}^{-1}) \quad (7)$$

Y-axis loading:

$$P_R = 404\ \text{N} + t_S\,(241\ \text{N mm}^{-1}) - M_S\,(17.4\ \text{N \%M}_{db}^{-1}) \quad (8)$$

Z-axis loading:

$$P_R = 356\ \text{N} + t_S\,(164\ \text{N mm}^{-1}) - M_S\,(13.0\ \text{N \%M}_{db}^{-1}) \quad (9)$$

where P_R is rupture force, t_S is shell thickness, M_S is shell moisture content, and $\%M_{db}$ is the moisture content unit of 1% dry basis. The standard errors associated with equations 7, 8, and 9 were 107, 118, and 126 N, respectively. Equations 7, 8, and 9 take the general form of equation 6, with the first two terms on the right side of the equation set equal to P_{max}, and the constant multiplied by M_S equal to R_M.

The significant differences in mean rupture force between the longitudinal (X-axis) loadings and those for lateral (Y-axis and Z-axis) loadings can be partly explained by nut growth characteristics and drying/wetting stresses, which differ in the longitudinal and lateral directions. Conversely, the significant difference in mean rupture force between Y-axis and Z-axis loadings (the two lateral loadings) can only be explained by differences in nut dimensions *B* and *C* and any variations in shell thickness that are aligned with dimensions *B* and *C*. Because, by definition, whole nut dimension *B* always exceeds dimension *C*, we would expect the mean rupture force, as measured in this study, to be significantly different for Y-axis and Z-axis loadings (fig. 9). In an attempt to account for this difference, the load aspect ratio was introduced into the regression analyses. The load aspect ratio (α) is herein defined as the ratio of the nut dimension parallel to the load axis to the average of the major and minor nut dimensions measured perpendicular to the load axis. In equation form:

$$\alpha = \alpha_X \text{ for X-axis loading} = 2A/(B + C) \quad (10)$$

$$\alpha = \alpha_Y \text{ for Y-axis loading} = 2B/(A + C) \quad (11)$$

$$\alpha = \alpha_Z \text{ for Z-axis loading} = 2C/(A + B) \quad (12)$$

Adding the load aspect ratio (α) as a variable in equations 7, 8, and 9 did not reduce the standard error of any of the axis-specific rupture force predictions. However, for combined Y-axis and Z-axis loading data, introduction of α into the rupture force model reduced the standard error from 134 to 126 N (a change significant at the 0.01 level) and

yielded the following equation:

Y-axis and Z-axis loadings:

$$P_R = 76\text{ N} + t_S\,(154\text{ N mm}^{-1}) + \alpha\,(398) - M_S\,(15.6\text{ N \%M}_{db}^{-1}) \quad (13)$$

Fracture surface area (A_F) was also explored as a possible predictor of rupture force. Fracture surface area is herein defined as the cross-sectional area exposed when a shell ruptures. For this investigation, fracture surface area was approximated as:

$$A_F = \pi[D_F^2 - (D_F - 2t_S)^2]/4 \quad (14)$$

where t_S is shell thickness, and D_F is the average of the major and minor diameters of the initial fracture plane. For Y-axis loadings, D_F was equated to $(A + B)/2$; for Z-axis loadings, D_F was set equal to $(A + C)/2$; and for X-axis loadings, D_F was taken as $(A + \min[B,C])/2$, where $\min[B,C]$ is the lesser of dimensions B and C. Inclusion of A_F in the predictive equations for rupture force due to Y-axis and Z-axis loadings did not reduce the standard errors over those associated with equations 8, 9, and 13. However, the following equation for X-axis loadings was associated with a standard error of a 101 N, a significant 6% decrease from that associated with equation 7:

X-axis loading:

$$P_R = 408\text{ N} + A_F\,(3.105\text{ N mm}^{-2}) - M_S\,(15.6\text{ N \%M}_{db}^{-1}) \quad (15)$$

Equation 13 for lateral (Y-axis and Z-axis) loadings and equation 15 for longitudinal (X-axis) loadings both show a moisture content reduction factor (R_M) for a rupture force of 15.6 N $\%M_{db}^{-1}$. This is approximately a 3% decrease in rupture force for every 1% increase in shell moisture content, dry basis.

On average, rupture forces for the hybrid hazelnuts in this study exceeded those reported for European cultivars and genotypes of *C. avellana*. This may be due to the thicker shells (relative to size) of hybrids of *C. americana*, but with no studies simultaneously reporting rupture force and shell thicknesses of European varieties, this cannot be verified. Of the European researchers, only Aydin (2002) and Güner et al. (2003) investigated the effect of moisture content on rupture force. Although those researchers also reported a reduction in rupture force with increased moisture content, the overall reduction was more on the order of 2% for each 1% increase in moisture content.

Rupture Energy

Mean rupture energy values for X-, Y-, and Z-axis loadings were 142, 249, and 229 N·mm, respectively (table 5). The mean value for X-axis loadings is significantly different at the 0.05 critical alpha level from the means for Y-axis and Z-axis loadings. However, the means for Y-axis and Z-axis loadings are not significantly different at the 0.05 critical alpha level. The coefficients of determination in table 5 indicate a weak positive correlation between rupture energy and shell thickness and a very weak positive correlation between rupture energy and geometric mean diameter. A somewhat stronger negative correlation exists between rupture energy and shell moisture content. This is in contrast with Güner et al. (2003), who showed a positive correlation between rupture energy and moisture content.

Initial and Secant Stiffness

Figures 4a and 4b illustrate compression tests characterized by a decrease and an increase, respectively, in stiffness with an increase in applied load. An increase in stiffness with an increase in applied load is characteristic of thin-shelled spheres that are compressed between parallel rigid plates (Taber, 1983; Updike and Kalnins, 1970, 1972; Shorter et al., 2010). The increase in stiffness occurs as the shell flattens against the surface of the flat plates.

The greater the extent to which shell flattening occurs prior to rupture, the more likely it is for secant stiffness to exceed initial stiffness. As shown in figure 17, secant stiffness exceeded initial stiffness 22%, 11%, and 55% of the time for X-, Y, and Z-axis loadings, respectively. The significant difference between the percentages for Y-axis and Z-axis loadings is explained by the fact that a Z-axis oriented nut (as shown in fig. 10) is easier to flatten. It follows that the lower the load aspect ratio (α), the more likely secant stiffness is to exceed initial stiffness. This statement is supported by the plot in figure 18 of K_S/K_I versus load aspect ratio for all 360 data points (i.e., combined data for X-, Y-, and Z-axis loadings).

The correlations in table 6 for initial stiffness and secant stiffness are similar, which can be expected given their sim-

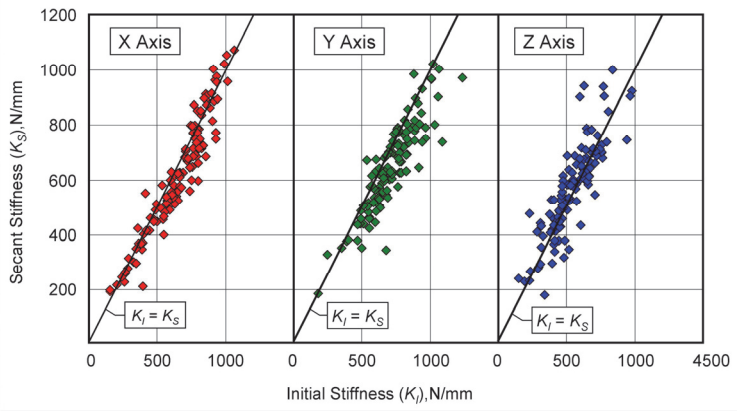

Figure 17. Relationship between secant stiffness and initial stiffness for each load axis.

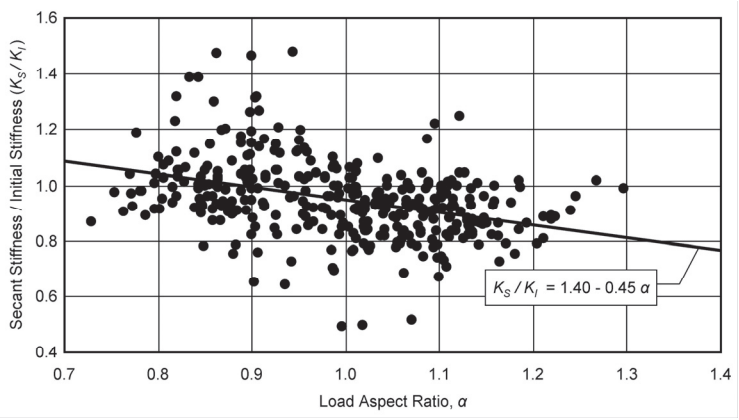

Figure 18. Secant stiffness versus initial stiffness as a function of load aspect ratio.

ilarity in magnitude. Overall, there is a significant negative correlation between stiffness and moisture content, and relatively weak positive correlations between stiffness and shell thickness and between stiffness and geometric mean diameter.

As with rupture force, the significant difference that load direction has on mean stiffness values (table 5) can be explained by differences in load aspect ratio (α). Overall, the following four-parameter equations were found to adequately predict initial stiffness and secant stiffness for all three load directions:

$$K_I = 178 \text{ N mm}^{-1} + t_S\,(86.0 \text{ N mm}^{-2}) + \alpha\,(596 \text{ N mm}^{-1}) - M_S\,(18.0 \text{ N (mm \%M}_{db})^{-1}) \quad (16)$$

$$K_S = 294 \text{ N mm}^{-1} + t_S\,(135 \text{ N mm}^{-2}) + \alpha\,(348 \text{ N mm}^{-1}) - M_S\,(17.9 \text{ N (mm \%M}_{db})^{-1}) \quad (17)$$

where K_I is initial stiffness, K_S is secant stiffness, t_S is shell thickness, α is load aspect ratio, and M_S is shell moisture content. The standard errors associated with equations 16 and 17 were 171 and 163 N mm^{-1}, respectively. The moisture reduction factors for initial stiffness and secant stiffness of 18.0 and 17.9 N (mm %M_{db})$^{-1}$, respectively, equate to slightly less than a 3% decrease in stiffness for every 1% increase in moisture content. This compares to a 1% to 2% decrease in the parallel-to-grain modulus of elasticity of wood for every 1% increase in moisture content, dry basis.

Nut Deformation at Rupture

As shown in table 5, loading direction was found to have a significant impact on nut deformation at rupture, with mean deformations at rupture of 0.66, 0.83, and 0.91 mm, respectively, for X-, Y-, and Z-axis loadings and associated standard deviations of 0.18, 0.21, and 0.33 mm, respectively. Cumulative frequency distribution and probability density curves for mean deformation at rupture (fig. 19) show the significant difference between X-axis (longitudinal) loadings and the Y-axis and Z-axis (lateral) loadings. Curves for the Y-axis and Z-axis loadings are nearly coincidental up to a cumulative frequency of 60%, at which point the curves begin to diverge, with the Z-axis loading curve exhibiting a longer right tail. This divergence explains the significant difference in mean deformation at rupture for Y-axis and Z-axis loadings, as well as the higher standard deviation for mean deformation at rupture for Z-axis loadings.

European researchers (Valentini et al., 2006; Ercisli et al., 2011) found that deformation at rupture for *C. avellana* also depended on load direction, and in the majority of cases also found rupture deformations for X-axis loadings to be less than those for Y-axis and Z-axis loadings. Overall, the magnitude of nut deformation at rupture was greater for *C. avellana* genotypes and cultivars than for the hybrids evaluated in this study. For example, nut deformation at rupture for longitudinal loadings reported by Ercisli et al. (2011) ranged between 1.16 and 1.76 mm for the 12 genotypes and cultivars they tested, with corresponding deformations for lateral loadings ranging between 1.14 and 1.54 mm.

Several relationships were investigated in an attempt to predict individual nut deformation at rupture from other hazelnut properties. These investigations included examination of the relationships between deformation at rupture and (1) shell moisture content, (2) geometric mean diameter, (3) shell thickness, (4) all three nut dimensions, and (5) load aspect ratio. Based on regression F-tests, none of the examined correlations were significant (and/or significant for all three load axes) at the 0.05 level. In regression equations featuring multiple independent variables, shell thickness showed a stronger correlation with nut deformation at rupture than did shell moisture content, geometric mean diameter, or load aspect ratio.

Of the cracking characteristics examined in this study, nut deformation at rupture is generally of greatest interest to hazelnut processors because the vast majority of cracking is accomplished by squeezing nuts between rollers that are a fixed distance apart (a.k.a. roller cracking). With a fixed spacing between the cracking rollers, the nuts must be sorted into size groups so that nuts in a particular group are not too large (as this results in kernel damage during cracking) nor too small (as this results in partially cracked and uncracked nuts). Because nuts tend to orient themselves with their longer dimensions parallel to the cracking roller surfaces, sorting for cracking rollers is typically done using devices with elongated openings (e.g., roller sorters) that sort according to the smallest dimension (i.e., S3) of the nut (fig. 9). It follows that when a nut orients itself with its longer dimension parallel to the cracking roller surfaces, the rollers apply a force parallel to the smallest dimension of the nut; that is,

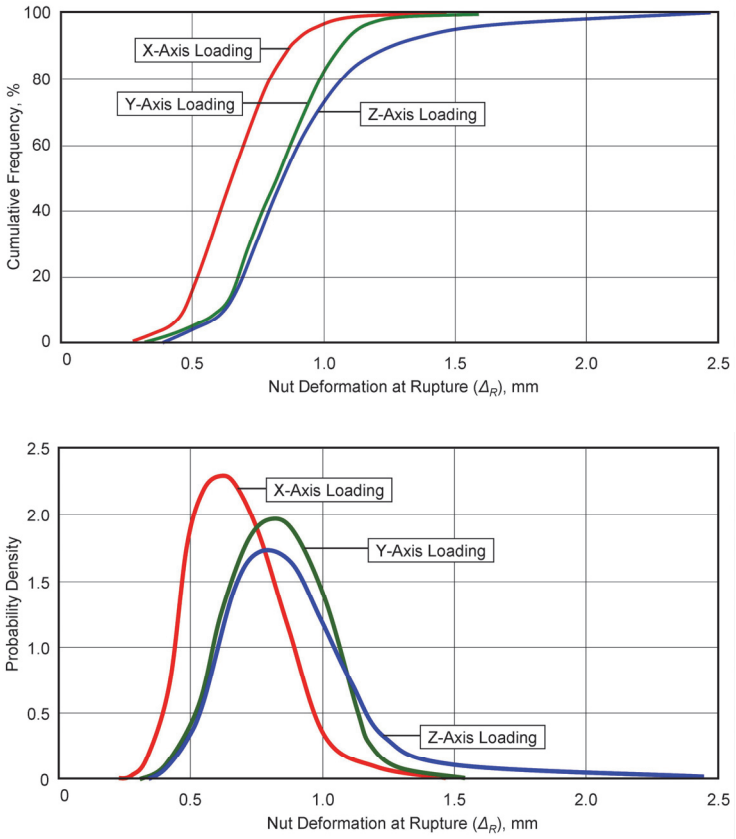

Figure 19. Cumulative frequency distribution and probability density curves for nut deformation at rupture for X-, Y-, and Z-axis loadings.

along the Z-axis when dimension *C* is the smallest dimension, and along the X-axis when dimension *A* is the smallest dimension. Because it is preferable to load nuts along their Z-axis, as this produces a better fracture than loading along the X-axis, nuts with dimension *C* as their smallest dimension (less oblate nuts) are more desirable for roller cracking.

Based on the curves in figure 19, it could be argued that nut pre-sizing for roller cracking should probably be in increments no greater than 0.3 or 0.4 mm, given that nut deformations of this magnitude will rupture some nuts. For each size group, the spacing between the cracking rollers could be established by reducing the roller spacing until approximately 10% of the nuts in the group are being cracked, and then reducing the spacing by about another 0.6 mm. Although this would not crack all nuts in the size group, it would hopefully avoid damage to kernels in nuts that are on the large end of the group.

Rupture Strain

The results for rupture strain mirror those for nut deformation at rupture. Whereas the correlations between rupture strain and shell thickness, moisture content, and geometric mean diameter were not considered significant (table 6), there were significant differences between the mean rupture strains of 4.4%, 5.4%, and 6.1% for the X-, Y-, and Z-axis loadings, respectively (table 5). Rupture strain of *C. avellana* was also shown by Güner et al. (2003) and Valentini et al. (2006) to depend on the axis of loading. However, the researchers reported significantly greater rupture strains for the European species. Specifically, rupture strains for the nine cultivars of *C. avellana* studied by Valentini et al. (2006) ranged from 4.4% to 9.8% for X-axis loadings, from 3.3% to 6.6% for Y-axis loadings, and from 5.2% to 11.8% for Z-axis loadings.

Kernel Density

The true density of hybrid hazelnut kernels was found to be 1000 kg m^{-3}. Aydin (2002) found the true density of European varieties of hazelnut kernel to be between 948 and 888 kg m^{-3}. Ozdemir and Akinci (2004) reported the true density of four major European varieties of hazelnut to range between 996 and 871 kg m^{-3}.

Conclusions

Physical properties of hybrid hazelnuts grown as seedlings in Wisconsin were measured and compared to previously published properties for *Corylus avellana* (European hazelnut).

- Geometric mean diameters of kernels and whole nuts were 10.2 and 14.8 mm, respectively. Published geometric mean diameters of European hazelnut kernels and whole nuts were larger by 3.9 and 4.6 mm, respectively.
- Sphericity values of kernels and whole nuts were 88.3% and 92.1%, respectively. Published sphericity values for European hazelnut kernels and whole nuts were slightly less at 87.7% and 90.0%, respectively.
- Larger hybrid hazelnuts tend to be more oblate than

smaller hazelnuts. The shape index of whole nuts increased by approximately 0.037 for every millimeter increase in geometric mean diameter.

- Almost without exception, when a nut is loaded, an initial crack forms along a longitudinal line parallel to the direction of applied load and then propagates rapidly until it has extended along two longitudinal lines (both parallel to the applied load), causing the shell to split into two pieces.
- Under lateral (Y-axis and Z-axis) loadings, the shell is split into nearly identical halves.
- At lower shell moisture contents, hazelnut shells fracture into more pieces.
- Shell thickness can vary significantly along a single longitudinal line, with a sharp decrease in thickness occurring at the poles. Shell thickness also varies around the equatorial plane and is thickest along the minor diameter of the equatorial plane.
- The mean rupture force was significantly lower for longitudinal (X-axis) loadings than for lateral (Y-axis and Z-axis) loadings. Rupture force for longitudinal loadings was best predicted with fracture area and moisture content as independent variables. Prediction of rupture force for lateral loadings was best predicted with shell thickness, load aspect ratio, and shell moisture content as independent variables. For all loadings, rupture force decreased by 15.6 N for every 1% increase in moisture content, dry basis.
- The mean rupture energy value of 0.142 J for X-axis loadings was significantly less than that for Y-axis loadings (0.249 J) and Z-axis loadings (0.229 J) at the 0.05 level. On average, rupture energy increased by 0.073 J for every millimeter increase in shell thickness and decreased by 0.007 J for every 1% increase in shell moisture content, dry basis.
- The mean initial stiffness and mean secant stiffness for all 360 whole nuts were 652 and 612 N mm^{-1}, respectively. Differences in mean stiffness values between load directions were adequately predicted with shell thickness, shell moisture content, and load aspect ratio as independent variables. Initial stiffness and secant stiffness decreased by approximately 18 N mm^{-1} for every 1% increase in moisture content, dry basis.
- The mean values of deformation at rupture of 0.66, 0.83, and 0.91 mm, respectively, for X-, Y-, and Z-axis loadings were significantly different at the 0.05 level. Correlations between nut deformation at rupture and shell thickness, shell moisture content, and geometric mean diameter were not considered significant. Published values of deformation at rupture for European hazelnuts are significantly greater than those for hybrid hazelnuts.
- Rupture strain values of 4.4%, 5.4%, and 6.1%, respectively, for X-, Y-, and Z-axis loadings were significantly different at the 0.05 level.
- True density of hybrid hazelnut kernels was found to be 1000 kg m^{-3}.

ACKNOWLEDGEMENTS

This research was supported in part by North Central Region Sustainable Agricultural Research and Education (NCR SARE) Grant NCR15-005: Commercialization of Hazelnuts for Growers in the Upper Midwest.

REFERENCES

ASABE. (2017). S368.4: Compression test of food materials of convex shape. St. Joseph, MI: ASABE.

Aydin, C. (2002). Postharvest technology: Physical properties of hazel nuts. *Biosyst. Eng., 82*(3), 297-303. https://doi.org/10.1006/bioe.2002.0065

Badgersett. (2015). Characteristics of Badgersett hybrid hazels. Canton, MN: Badgersett Research Corporation. Retrieved from http://www.badgersett.com/info/hazelnuts/hazel2.html

Bohnhoff, D. R. (2017). Apparatus for rapid material moisture conditioning using saturated salt solutions. ASABE Paper No. 1700663. St. Joseph, MI: ASABE. https://doi.org/10.13031/aim.201700663

Bohnhoff, D. R., & Bohnhoff, R. K. (2019). Equilibrium moisture content of hazelnut husks, shells, and kernels. *Trans. ASABE, 62*(5), 1075-1086. https://doi.org/10.13031/trans.13257

Braun, L. C., Demchik, M., Fischbach, J., Turnquist, K., & Kern, A. J., (2019). Yield, quality, and genetic diversity of hybrid hazelnut selections in the Upper Midwest of the USA. *Agroforestry Syst., 93*(3), 1081-1091 https://doi.org/10.1007/s10457-018-0209-7

Delprete, C., & Sesana, R. (2014). Mechanical characterization of kernel and shell of hazelnuts: Proposal of an experimental procedure. *J. Food Eng., 124*, 28-34. https://doi.org/10.1016/j.jfoodeng.2013.09.027

Delprete, C., Giacosa, S., Raviolo, E., Rolle, L., & Sesana, R. (2015). Experimental characterization and numerical modeling of the compressive mechanical behavior of hazelnut kernels. *J. Food Eng., 166*, 364-369. https://doi.org/10.1016/j.jfoodeng.2015.06.037

Ercisli, S., Ozturk, I., Kara, M., Kalkan, H., Seker, H., Duyar, O., & Erturk, Y. (2011). Physical properties of hazelnuts. *Intl. Agrophys., 25*, 115-121.

Fischbach, J. A., & Tibbals, K. (2016). Hybrid hazelnut production trials: Year 5 yield and performance. Madison, WI: University of Wisconsin, Extension Bayfield County.

FPL. (2010). Wood handbook: Wood as an engineering material. FPL-GTR-190. Madsion, WI: USDA Forest Service, Forest Products Laboratory. Retrieved from http://www.fpl.fs.fed.us/documnts/fplgtr/fpl_gtr190.pdf

Güner, M., Dursun, E., & Dursun, I. G. (2003). Mechanical behaviour of hazelnut under compression loading. *Biosyst. Eng., 85*(4), 485-491. https://doi.org/10.1016/S1537-5110(03)00089-8

Lawson, K. S., Bohnhoff, D. R., & Fischbach, J. A. (2018). Physical properties of Upper Midwest USA grown hybrid hazelnuts. ASABE Paper No. 1800031. St. Joseph, MI: ASABE. https://doi.org/10.13031/aim.201800031

Ozdemir, F., & Akinci, I. (2004). Physical and nutritional properties of four major commerical Turkish hazelnut varieties. *J. Food Eng., 63*(3), 341-347. https://doi.org/10.1016/j.jfoodeng.2003.08.006

Palipane, K. B., & Driscoll, R. H. (1992). Moisture sorption characteristics of in-shell macadamia nuts. *J. Food Eng., 18*(1), 63-76. https://doi.org/10.1016/0260-8774(93)90075-U

R Development Team. (2016). R: A language and environment for statistical computing. Vienna, Austria: R Foundation for Statistical Computing. Retrieved from http://www.r-project.org/

Shorter, R., Smith, J. D., Coveney, V. A., & Busfield, J. C. (2010).

Axial compression of hollow elastic spheres. *J. Mech. Mater. Struct., 5*(5), 693-705. https://doi.org/10.2140/jomms.2010.5.693

Taber, L. A. (1983). Compression of fluid-filled spherical shells by rigid indenters. *J. Appl. Mech., 50*(4a), 717-722. https://doi.org/10.1115/1.3167135

Updike, D. P., & Kalnins, A. (1970). Axisymmetric behavior of an elastic spherical shell compressed between rigid plates. *J. Appl. Mech., 37*(3), 635-640. https://doi.org/10.1115/1.3408592

Updike, D. P., & Kalnins, A. (1972). Axisymmetric postbuckling and nonsymmetric buckling of a spherical shell compressed between rigid plates. *J. Appl. Mech., 39*(1), 172-178. https://doi.org/10.1115/1.3422607

Valentini, N., Rolle, L., Stevigny, C., & Zeppa, G. (2006). Mechanical behaviour of hazelnuts used for table consumption under compression loading. *J. Sci. Food Agric., 86*(8), 1257-1262. https://doi.org/10.1002/jsfa.2486